Three-dimensional nonperturbative analysis of spontaneous emission in a Fabry-Perot microcavity

Ho Trung Dung* and Kikuo Ujihara
The University of Electro-Communications, 1-5-1 Chofugaoka, Chofu, Tokyo 182-8585, Japan
(Received 10 December 1998; revised manuscript received 16 June 1999)

A three-dimensional quantum nonperturbative theory of spontaneous emission in a planar microcavity is developed on the basis of a complete set of orthogonal standing-wave mode functions. Earlier results on the spontaneous decay rate and far-field emission pattern which have been obtained in a perturbative fashion are shown to be contained in our theory. Time evolution of the initially excited atomic state is considered and comparison with perturbative results is given. It is found that though the Fabry-Perot cavity is of an open type, vacuum-field Rabi oscillations are still possible. Conditions that are favorable for this strong coupling regime are discussed. The near-field spontaneous-emission pattern and the transition from the near field to the far field are investigated. For moderate mirror reflectivities, the spread in the near-field emission pattern is found to be in good agreement with the effective mode radius concept. When the mirror reflectivity increases, however, one has a strong coupling regime and together with it, multiple reabsorptions and reemissions of the photon may occur, leading to a better localization of the photon around the atomic position. These considerations may be useful in designing microlasers of the planar type. [S1050-2947(99)03211-4]

PACS number(s): 42.50.Ct, 42.60.−v

I. INTRODUCTION

It is now understood that spontaneous emission from an atom is very sensitive to the mode density and mode structure of the surrounding environment in which the atom is radiating. The spontaneous-emission rate can be either increased or decreased as compared to its free-space value and the emission pattern may become highly anisotropic [1–3]. There are also similar effects in the spontaneous emission from recombining electron-hole pairs or excitons in semiconductors, where tailoring the spontaneous emission holds technological promise for realizing thresholdless, high-speed modulation microlasers [1,4–7].

An important class of material media configurations in which the active optical material is embedded are the planar Fabry-Perot cavities. This type of cavity configuration has attracted a great deal of attention due to simple fabrication technology and due to the fact that it lends itself relatively easily to analytical considerations [8–27]. Various aspects of the spontaneous-emission process including the spontaneous emission rate and the spontaneous emission pattern have been studied. These treatments, however, are mainly within the framework of Fermi's golden rule and do not accommodate the strong coupling effects such as vacuum-field Rabi oscillations [28] and vacuum-field Rabi splittings [29]. Nonperturbative multi-mode treatments have been carried out only for one-dimensional models [23–27].

In this paper we present a three-dimensional nonperturbative analysis of spontaneous emission in a planar cavity with symmetrical two-side output coupling, based on a multimode description of the electromagnetic field. There are many reasons why such a study is desirable. First, although a one-dimensional theory can describe adequately many aspects of spontaneous emission in a planar cavity, it is far from realistic because an important channel of photon loss, the emission into oblique modes, is neglected. Besides, problems such as spatial distribution of spontaneous emission cannot be addressed. Second, though when the atom-radiation coupling is weak, the spontaneous-emission process can be well approximated using a perturbation theory, this weak coupling regime will be justified to various extents depending on factors such as the cavity length, the atomic position and atomic dipole orientation. It is therefore important to clarify how well the perturbation theory works under different circumstances. Third, though it has been argued intuitively before that since a planar cavity confines the field in only one spatial dimension, there are no Rabi oscillations [21], we believe that only a nonperturbative theory which takes into account properly the cavity mode structure can give an ultimate answer to this question. And as we shall show below, vacuum-field Rabi oscillations, though rather weak and fragile, can still appear and may lead to important physical implications. Fourth, while earlier works on the spontaneous-emission pattern have been restricted to perturbative calculations of the far field [15,16,18–21], or of the field intensity along a line normal to the mirrors passing through the atom [17], we aim here at giving a comprehensive treatment of the spatial emission pattern including both near and far fields and weak and strong coupling regimes. By examining the near-field pattern, we can also gain further insights into the concept of transverse quantum correlation length introduced by De Martini *et al.* [30] or, equivalently, the concept of effective mode radius introduced by Ujihara [15,31]. Finally, we hope that our results could be utilized for practical purposes, e.g., in designing the vertical cavity surface emitting lasers [32].

The paper is organized as follows. In Sec. II, the cavity model and mode functions are given. We start out by calcu-

*On leave from the Institute of Physics, National Center for Sciences and Technology, 1 Mac Dinh Chi St., Dist. 1, Ho Chi Minh City, Vietnam.

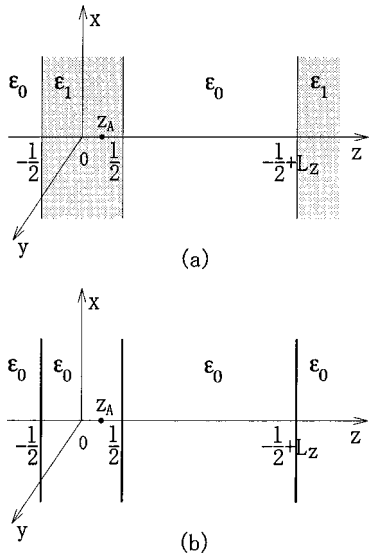

FIG. 1. (a) is the single dielectric slab configuration which serves as a starting point for our derivation of the mode functions. The symmetrical Fabry-Perot cavity with two infinitely thin and semitransparent mirrors shown in (b) is the one we actually use in our calculations.

lating the standing-wave mode functions for a single dielectric slab and after applying an appropriate limiting procedure, reduce them to those of a Fabry-Perot cavity with two similar infinitely thin, semitransparent, and absorptionless mirrors. In Section III, these mode functions are shown to reproduce exactly the same perturbative results on the spontaneous-emission rate obtained previously by using the alternative traveling-wave mode functions for symmetrical cavities [17], including the case of two perfectly reflecting mirrors [3,11–13]. Next we derive a delay-differential equation for the time evolution of the atomic upper-state probability amplitude and obtain an analytic solution to it for the particular case where the atom is at the cavity center. Transient behavior of the atomic upper-state population is studied numerically and compared with that predicted by Fermi's golden rule. It is shown, in particular, that strong coupling regime can be achieved in a one half wavelength cavity, with the atom at the antinode position and atomic dipole parallel to the cavity mirrors, provided that there is a high enough cavity finesse or a large enough dipole matrix element. The spontaneous emission pattern is investigated in Sec. IV, where the near-field and far-field patterns are calculated in both weak and strong coupling regimes. Conclusions are given in Sec. V, and lengthy mathematical derivations are outlined in the Appendices.

II. CAVITY MODEL AND MODE FUNCTIONS

Let us start by considering a single nondispersive planar dielectric slab of thickness l and dielectric constant ϵ_1, embedded in a vacuum of dielectric constant ϵ_0. The coordinate system is chosen such that the z axis is normal to the dielectric slab surface with its origin in the middle of the slab. The dielectric slab is assumed to have infinite extents in the xy plane and a two-level atom with the transition frequency ω_A and dipole matrix element $\boldsymbol{\mu}$ is placed inside the cavity at $\mathbf{r}_A=(0,0,z_A)$, see Fig. 1(a). The electromagnetic field is expanded in terms of orthogonal field mode functions $\mathbf{U}_j(\mathbf{r})$ defined by imposing periodic boundary conditions in x, y, and z directions with periods L_x, L_y, and L_z, respectively. They are normalized so that

$$\int_V \epsilon(\mathbf{r})\mathbf{U}_i(\mathbf{r})\mathbf{U}_j(\mathbf{r})d\mathbf{r}=\delta_{ij},$$

where $V=L_xL_yL_z$. The mode functions in the dielectric and in the vacuum are denoted by $\mathbf{U}_1$ and $\mathbf{U}_0$, respectively, and will be given in terms of relevant mode wave vectors $\mathbf{k}_{1,0}=(k_x,k_y,k_{1,0z})$ for inside and outside the cavity and their projections onto the xy plane $\mathbf{k}_p=(k_x,k_y,0)$ beside the mode index j. The mode functions are categorized into TE and TM mode functions of even and odd symmetries in the z direction. They are further categorized into even and odd functions in the x-y direction. The odd-x-y TE mode functions read [31]

$$\mathbf{U}_{1,0}(\mathbf{r})=\alpha(\hat{x}k_y-\hat{y}k_x)\sin(\mathbf{k}_p\cdot\mathbf{r})u_{1,0}(z), \tag{1}$$

where $u_{1,0}(z)$ and the normalization constant α are, for odd-z TE modes,

$$u_1^{\mathrm{ozTE}}(z)=\sin k_{1z}z, \tag{2a}$$

$$u_0^{\mathrm{ozTE}}(z)=\sin\frac{k_{1z}l}{2}\cos k_{0z}\left(z-\frac{l}{2}\right)+\frac{k_{1z}}{k_{0z}}\cos\frac{k_{1z}l}{2}\sin k_{0z}\left(z-\frac{l}{2}\right), \tag{2b}$$

$$\alpha^{\mathrm{ozTE}}=\frac{2}{\sqrt{\epsilon_0 V}}\frac{1}{k_p}\frac{k_{0z}}{k_{1z}}\left[1-\left(1-\frac{k_{0z}^2}{k_{1z}^2}\right)\sin^2\frac{k_{1z}l}{2}\right]^{-1/2}, \tag{3}$$

and, for even-z TE modes,

$$u_1^{\mathrm{ezTE}}(z)=\cos k_{1z}z, \tag{4a}$$

$$u_0^{\mathrm{ezTE}}(z)=\cos\frac{k_{1z}l}{2}\cos k_{0z}\left(z-\frac{l}{2}\right)-\frac{k_{1z}}{k_{0z}}\sin\frac{k_{1z}l}{2}\sin k_{0z}\left(z-\frac{l}{2}\right), \tag{4b}$$

$$\alpha^{\mathrm{ezTE}}=\frac{2}{\sqrt{\epsilon_0 V}}\frac{1}{k_p}\frac{k_{0z}}{k_{1z}}\left[1-\left(1-\frac{k_{0z}^2}{k_{1z}^2}\right)\cos^2\frac{k_{1z}l}{2}\right]^{-1/2}. \tag{5}$$

The even-x-y TE mode functions are obtained by replacing $\sin(\mathbf{k}_p\cdot\mathbf{r})$ by $\cos(\mathbf{k}_p\cdot\mathbf{r})$ in Eq. (1). The TM mode functions for odd-x-y modes are

$$\mathbf{U}_{1,0}(\mathbf{r})=\alpha\left[(\hat{\mathbf{x}}k_x+\hat{\mathbf{y}}k_y)\sin(\mathbf{k}_p\cdot\mathbf{r})\frac{d}{dz}u_{1,0}(z)-\hat{\mathbf{z}}k_p^2\cos(\mathbf{k}_p\cdot\mathbf{r})u_{1,0}(z)\right], \tag{6}$$

where $u_{1,0}(z)$ and the normalization constant α are, for even-z TM modes,

$$u_1^{\mathrm{ezTM}}(z)=\cos k_{1z}z, \tag{7a}$$

$$u_0^{\mathrm{ezTM}}(z)=\cos\frac{k_{1z}l}{2}\cos k_{0z}\left(z-\frac{l}{2}\right)$$

$$-\frac{k_{1z}k_0^2}{k_{0z}k_1^2}\sin\frac{k_{1z}l}{2}\sin k_{0z}\left(z-\frac{l}{2}\right), \tag{7b}$$

$$\alpha^{\mathrm{ezTM}}=\frac{2}{\sqrt{\epsilon_0 V}}\frac{1}{k_p k_0}\frac{k_{0z}k_1^2}{k_{1z}k_0^2}\left[1-\left(1-\frac{k_{0z}^2k_1^4}{k_{1z}^2k_0^4}\right)\cos^2\frac{k_{1z}l}{2}\right]^{-1/2}, \tag{8}$$

and, for odd-z TM modes,

$$u_1^{\mathrm{ozTM}}(z)=\sin k_{1z}z, \tag{9a}$$

$$u_0^{\mathrm{ozTM}}(z)=\sin\frac{k_{1z}l}{2}\cos k_{0z}\left(z-\frac{l}{2}\right)$$

$$+\frac{k_{1z}k_0^2}{k_{0z}k_1^2}\cos\frac{k_{1z}l}{2}\sin k_{0z}\left(z-\frac{l}{2}\right), \tag{9b}$$

$$\alpha^{\mathrm{ozTM}}=\frac{2}{\sqrt{\epsilon_0 V}}\frac{1}{k_p k_0}\frac{k_{0z}k_1^2}{k_{1z}k_0^2}\left[1-\left(1-\frac{k_{0z}^2k_1^4}{k_{1z}^2k_0^4}\right)\sin^2\frac{k_{1z}l}{2}\right]^{-1/2}, \tag{10}$$

while the even-x-y TM modes are obtained by replacing $\sin(\mathbf{k}_p\cdot\mathbf{r})$ in front of $(d/dz)u_{1,0}(z)$ by $\cos(\mathbf{k}_p\cdot\mathbf{r})$ and $-\cos(\mathbf{k}_p\cdot\mathbf{r})$ in front $u_{1,0}(z)$ by $\sin(\mathbf{k}_p\cdot\mathbf{r})$. Note that the mode functions in Eqs. (1)–(10) describe standing waves rather than traveling waves and in these equations, we have suppressed the mode index j.

It is convenient to write the normalization constants α in terms of Fourier series

$$(\alpha^{\mathrm{ezTE}})^2=\frac{4}{\epsilon_0 V}\frac{1}{k_p^2}\frac{k_{0z}}{k_{1z}}\left[1+2\sum_{n=1}^{\infty}r^n\cos(k_{1z}nl)\right], \tag{11}$$

$$r=\frac{k_{1z}-k_{0z}}{k_{1z}+k_{0z}}, \tag{12}$$

$$(\alpha^{\mathrm{ozTM}})^2=\frac{4}{\epsilon_0 V}\frac{1}{k_p^2k_0^2}\frac{k_{0z}k_1^2}{k_{1z}k_0^2}\left[1+2\sum_{n=1}^{\infty}r'^n\cos(k_{1z}nl)\right], \tag{13}$$

$$r'=\frac{k_{0z}k_1^2-k_{1z}k_0^2}{k_{0z}k_1^2+k_{1z}k_0^2}. \tag{14}$$

Similar expansions for odd-z TE and even-z TM modes are obtained by replacing r and r' by $-r$ and $-r'$, respectively.

In further calculations below, for simplicity, we shall make the dielectric constant ϵ_1 of the dielectric slab equal to the vacuum dielectric constant ϵ_0, but keep the reflectivities in the Fourier expansions (11) and (13) finite. That is, we set $\epsilon_1\to\epsilon_0$ and $k_1\to k_0\equiv k$ with r and r' finite. We also assume that $r=r'$ and that they are independent of the k-vector orientation. These assumptions reduce our cavity model to that of a pair of infinitely thin mirrors with vacuum inner space; the mirrors are lossless and have a mode independent reflectivity, see Fig. 1(b). Similar cavity models have also been employed in earlier treatments [17].

III. TIME EVOLUTION OF THE ATOMIC-STATE POPULATIONS

A. Nonperturbative solution

With the mode functions in hand, the electromagnetic field can be quantized in a standard manner and the Hamiltonian which describes the atom–radiation-field system reads, in the electric dipole and rotating-wave approximations,

$$\hat{H}=\sum_j\hbar\omega_j\hat{a}_j^\dagger\hat{a}_j+\hbar\omega_{\mathrm{A}}\hat{b}_u^\dagger\hat{b}_u+\hbar\sum_j(\kappa_j\hat{\sigma}^\dagger\hat{a}_j+\kappa_j^*\hat{a}_j^\dagger\hat{\sigma}), \tag{15}$$

with the coupling constant

$$\kappa_j=-i\sqrt{\frac{\omega_j}{2\hbar}}\mathbf{U}_j(\mathbf{r}_{\mathrm{A}})\cdot\boldsymbol{\mu}\ . \tag{16}$$

Here $\hat{a}_j^\dagger$ and $\hat{a}_j$ are the creation and annihilation operators of the field mode j with mode frequency ω_j, while $\hat{b}_i^\dagger$ and $\hat{b}_i$ $(i=u,l)$ are the creation and annihilation operators of the upper and lower states of the emitting two-level atom. The atomic flopping operators are defined as $\hat{\sigma}=\hat{b}_l^\dagger\hat{b}_u$ and $\hat{\sigma}^\dagger=\hat{b}_u^\dagger\hat{b}_l$. We assume that the atom is initially excited and there is no photon in the radiation field so that the system wave function in the Schrödinger picture can be written as

$$|\psi(t)\rangle=C_u(t)e^{-i\omega_{\mathrm{A}}t}|u\rangle|\{0\}\rangle+\sum_j C_{lj}(t)e^{-i\omega_j t}|l\rangle|\{1_j\}\rangle, \tag{17}$$

where $|\{0\}\rangle$ denotes the vacuum state of the radiation field and $|\{1_j\}\rangle$ denotes the field state where there is one photon in mode j and no photon in all other modes. The Schrödinger equation yields

$$\dot{C}_u(t)=-i\sum_j\kappa_jC_{lj}(t)e^{-i(\omega_j-\omega_{\mathrm{A}})t}, \tag{18}$$

$$\dot{C}_{lj}(t)=-i\kappa_j^*C_u(t)e^{i(\omega_j-\omega_{\mathrm{A}})t}. \tag{19}$$

Taking into account the fact that initially $C_{lj}(0)=0$, Eq. (19) can be formally integrated and put into Eq. (18) to give

$$\dot{C}_u(t)=\int_0^t K(t-t')C_u(t')dt', \tag{20}$$

where the kernel $K(t-t')$ is defined as

$$K(t-t')=-\sum_j|\kappa_j|^2e^{-(\omega_j-\omega_{\mathrm{A}})(t-t')}\ . \tag{21}$$

By using Eq. (16) and the mode functions given in Sec. II and replacing the sum over the mode index j by an integral, this kernel can be calculated (see Appendix A) and put in Eq. (20) to yield

$$\dot{C}_u(t) = -\frac{A_0}{2}C_u(t) + \sum_{n=1}^{\infty} p_{2n}(\omega_A nT)C_u(t-nT)H(t-nT)$$
$$+\frac{1}{2}\sum_{n=0}^{\infty}\{p_{2n+1}[\omega_A(nT+t_r)]C_u(t-nT-t_r)$$
$$\times H(t-nT-t_r)+p_{2n+1}[\omega_A(nT+t_l)]$$
$$\times C_u(t-nT-t_l)H(t-nT-t_l)\}, \quad (22)$$

where $H(x)$ is the Heaviside unit step function;

$$A_0 = \frac{\mu^2\omega_A^3}{3\pi\epsilon_0\hbar c^3} \quad (23)$$

is the free-space decay rate; and

$$T = \frac{2l}{c}, \quad t_r = \frac{l-2z_A}{c}, \quad t_l = \frac{l+2z_A}{c} \quad (24)$$

are the round-trip travel time of a photon in the cavity, the time for a photon to travel from the atomic position to the right mirror and back, and the time for a photon to travel from the atomic position to the left mirror and back, respectively. The coefficients $p_n(x)$ can be either $p_n^{\parallel}$ when the dipole is oriented parallel to the mirror surfaces or $p_n^{\perp}$ when the dipole is oriented perpendicular to the mirror surfaces

$$p_n^{\parallel}(x) = -\frac{3A_0}{2}r^n\left(\frac{1}{ix}+\frac{1}{x^2}-\frac{1}{ix^3}\right)e^{ix}, \quad (25a)$$

$$p_n^{\perp}(x) = 3A_0(-r)^n\left(\frac{1}{x^2}-\frac{1}{ix^3}\right)e^{ix}. \quad (25b)$$

Clearly, any other dipole orientation can be treated as a linear superposition of the above two cases. The delay-differential equation (22) is the three-dimensional version of that obtained earlier for one-dimensional planar cavities [23–25]. Its first term stems from a natural decay in a free space while the others describe the back action of light reflected at the cavity walls on the atom with correct retardation times. These reflections can also be interpreted as the effects of the atomic mirror images on the spontaneous emission process [33–35]. As compared with the one-dimensional case, $p_n(x)$ now has a more complicated structure displaying x^{-1}-, x^{-2}-, and x^{-3}-terms which, as in usual dipolar radiation [36,37], correspond to the dipole radiation field, the induced field, and the electrostatic field, respectively, due to the mirror images. The absence of the x^{-1}-term in Eq. (25b) is because the mirror-image dipoles are pointing towards the original atom and cannot contribute a dipole radiation term to the atom.

When the atom is positioned at the cavity center ($z_A = 0$), the three series in Eq. (22) can be combined leading to a simpler delay-differential equation

$$\dot{C}_u(t) = -\frac{A_o}{2}C_u(t) + \sum_{n=1}^{\infty} p_n(k_A nl)C_u(t_n)H(t_n) \quad (26)$$

with

$$t_n \equiv t - \frac{nl}{c}. \quad (27)$$

This equation can be solved analytically (see Appendix B) to yield

$$C_u(t) = \sum_{n=0}^{\infty}\left[\sum \frac{p_1^{a_1}(k_A l)p_2^{a_2}(k_A 2l)\cdots p_n^{a_n}(k_A nl)}{a_1!a_2!\cdots a_n!}\right.$$
$$\left.\times t_n^m \exp\left(-\frac{A_0}{2}t_n\right)\right]H(t_n), \quad (28)$$

where the inner sum is over all non-negative integers a_i ($i = 1,2,\cdots,n$) such that

$$1a_1 + 2a_2 + \cdots + na_n = n$$

and

$$m = a_1 + a_2 + \cdots + a_n.$$

Note that the ''method of steps'' employed in Appendix B to solve the delay-differential equation (26) is also applicable, e.g., in the problem of two atoms at a fixed distance apart in a free space, where retardation plays an important role in the atom-radiation interaction process [38].

When the atom is off the cavity center, the general delay-differential equation (22) has to be integrated numerically. In order to compare our results with perturbative ones, we now turn to the perturbation theory.

B. Cavity modified spontaneous-emission rate and relation to earlier works

Perturbative results can be obtained by ignoring the unit step functions and replacing $C_u(t)$ on the right-hand side of Eq. (22) by its initial value $C_u(0) = 1$. Hence from the relationship

$$\Gamma = -\frac{d}{dt}|C_u(t)|^2, \quad (29)$$

we get the following expression for the cavity modified spontaneous-emission rate

$$\Gamma = A_0 - 2\mathrm{Re}\sum_{n=1}^{\infty} p_{2n}(\omega_A nT) - \mathrm{Re}\sum_{n=0}^{\infty}\{p_{2n+1}[\omega_A(nT+t_r)]$$
$$+ p_{2n+1}[\omega_A(nT+t_l)]\}, \quad (30)$$

where $p_n(x)$ is defined in Eqs. (25). It is not difficult to verify that the same result can be obtained directly from the Fermi's golden rule

$$\Gamma = \sum_j \frac{\pi\omega_j}{\hbar}|\mathbf{U}_j(\mathbf{r}_A)\cdot\boldsymbol{\mu}|^2\delta(\omega_j - \omega_A). \quad (31)$$

Our derivation, however, elucidates more clearly the Markovian conditions assumed for the perturbative calculation, under which the future of the system is determined by the present and not its past.

To show that previous perturbative results are contained in our theory, it is helpful first to rewrite the normalization constants α as

$$(\alpha^{\mathrm{ezTE}})^2=\frac{4}{\epsilon_0 V}\frac{1}{k_p^2}\frac{k_{0z}}{k_{1z}}\frac{(1+r)^2-4r\sin^2(k_{1z}l/2)}{1-r^2+4(r^{-2}-1)^{-1}\sin^2 k_{1z}l}, \tag{32}$$

$$(\alpha^{\mathrm{ozTM}})^2=\frac{4}{\epsilon_0 V}\frac{1}{k_p^2 k_0^2}\frac{k_{0z}k_1^2}{k_{1z}k_0^2}\frac{(1+r')^2-4r'\sin^2(k_{1z}l/2)}{1-r'^2+4(r'^{-2}-1)^{-1}\sin^2 k_{1z}l}. \tag{33}$$

Similar expressions for odd-z TE and even-z TM modes can be obtained from Eqs. (32) and (33), respectively, by replacing $\sin(k_{1z}l/2)$ in the numerators by $\cos(k_{1z}l/2)$. Substituting the mode functions with the normalization constants in the form (32) and (33) into the Fermi's golden rule (31), after letting $\epsilon_1\rightarrow\epsilon_0$, $k_1\rightarrow k_0\equiv k$ while keeping $r=r'$ finite, and replacing the summation over the mode index by an integral as in Eq. (A1), we arrive at

$$\Gamma=\frac{3A_0}{4}\int_0^1 dC(1+C^2)G(C), \tag{34}$$

where

$$G^{\parallel}(C)=\frac{(1+r)^2-2r\{\sin^2[k_{\mathrm{A}}C(l/2+z_{\mathrm{A}})]+\sin^2[k_{\mathrm{A}}C(l/2-z_{\mathrm{A}})]\}}{1-r^2+4(r^{-1}-1)^{-1}\sin^2(k_{\mathrm{A}}Cl)}, \tag{35a}$$

$$G^{\perp}(C)=\frac{(1+r)^2-2r\{\cos^2[k_{\mathrm{A}}C(l/2+z_{\mathrm{A}})]+\cos^2[k_{\mathrm{A}}C(l/2-z_{\mathrm{A}})]\}}{1-r^2+4(r^{-1}-1)^{-1}\sin^2(k_{\mathrm{A}}Cl)}, \tag{35b}$$

i.e., in full agreement with Eqs. (4.15)–(4.17) obtained by De Martini and co-workers using the traveling-wave mode functions [17]. For a high Q-cavity, the denominators in Eqs. (35) can be expressed as sums of δ-functions and the integral in Eq. (34) can be performed in closed form, leading to a spontaneous emission rate which is consistent with the results derived previously for a cavity with perfectly reflecting mirrors [3,11,12,17,20]. With these preliminary steps in hand, we can now move on to numerical calculations.

C. Numerical results

In our numerical study, we shall assume a cos-type cavity for which $r<0$ and a relatively high cavity finesse. Though for completeness formulas for both cases of the dipole orientations (parallel and perpendicular to the cavity walls) are given, we shall focus on the first. Since a dipole is coupled most strongly to the electric field parallel to its direction [39], a dipole parallel to the mirror surfaces will be coupled preferably to the longitudinal modes and is expected to bring out the cavity effects most pronouncedly. This is also a good approximation for the models where the dipole moment originates from an electron and a heavy hole in a thin semiconductor quantum well oriented in the xy-plane, which are of considerable practical interest [1].

The atomic upper state population is plotted in Fig. 2 as a function of the dimensionless time $t/(\lambda/c)$ for different values of the scaled cavity length

$$m=\frac{l}{\lambda/2}.$$

The atom is placed in the middle of the cavity and we have taken $r=-0.99$, $A_0\lambda/(2c)=10^{-3}$–a value that can be realized using an atomic transition in the optical domain. Both nonperturbative (bold curves) and perturbative (light curves) results are presented.

From Fig. 2 it can be seen that while the perturbative theory works satisfactorily for small times and for $m=2$, it deviates from the nonperturbative one at larger times for $m=1$ and $m=3$. This can be easily understood taking into account the fact that the atom-field coupling is weak at a node position (even m) and is stronger at an antinode position (odd m). We also observe that the disagreement between the perturbative and nonperturbative approaches which occurs for odd values of m tends to vanish with an

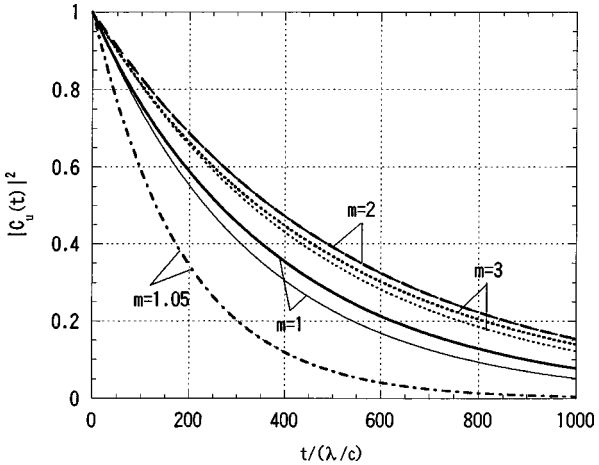

FIG. 2. Time evolution of the atomic upper-state population for different values of the scaled cavity length $m=l/(\lambda/2)$. Nonperturbative results are represented by bold curves and perturbative ones by light curves. The atom is placed at the cavity center and has its dipole oriented parallel to the mirror surfaces. Other parameters are $A_0\lambda/(2c)=10^{-3}$ and $r=-0.99$.

increase of the cavity length, i.e., when we move from a well-confined space toward a free space. Another special case of interest is when the cavity gap is slightly longer than one half wavelength. At this point maximum spontaneous-emission enhancement is achieved [20] and one might naively suggest that the discrepancy between the nonperturbative and perturbative results would be at its largest. However, our numerical results for $m=1.05$ show that that is not the case. The reason lies in the emission pattern. As we shall show in the next section, in the case of $m=1.05$, the near-field emission pattern is broader and its intensity on the z-axis is weaker than those in the case of $m=1$ and as a consequence, light is emitted mostly into oblique directions and cannot act back on the atom after being reflected.

What we see in Fig. 2 is clearly the weak coupling regime. The weak and strong coupling regimes can be distinguished by the relationship among the three coupling constants: the dipole coupling constant κ between the atom and the resonant cavity mode, the decay rate γ_c of this mode via mirror losses, and the rate γ' of spontaneous emission into a continuum of vacuum modes present when the cavity is open-sided [40,41]. A weak coupling regime takes place when the irreversible decay rates γ_c and γ' dominate over the atom-cavity mode dipole interaction: $\gamma_c,\ \gamma' \gg \kappa$, whereas the strong coupling regime occurs when the coherent interaction between the atom and the cavity mode dominates over the irreversible decay mechanisms: $\kappa \gg \gamma_c, \gamma'$. In contrast to [40,41], where the three coupling constants have been introduced somewhat arbitrarily, without specifying the cavity configuration, in our case of a Fabry-Perot cavity, they are defined automatically by the mode functions, the atomic position and dipole orientation. We shall compare them directly in the next section and give here instead a qualitative argument as follows. It is physically obvious that in order to facilitate a strong coupling regime we have to reduce the atomic emission into the oblique directions, that is, to minimize γ'. This can be achieved to a certain extent by choosing a dipole orientation parallel to the mirror surfaces, putting the atom at an antinode position, and narrowing the cavity gap to one half wavelength. Further we need a large $A_0\lambda/(2c)$, which means a large coherent coupling strength κ at a given transition frequency, or a large mirror reflectivity, which means a smaller cavity damping rate γ_c, or both. A relationship between γ_c and r can be established by expanding the normalization constants α in accordance with the Mittag-Lefler theorem [25,42]

$$\gamma_c = \frac{2}{T}\ln\left(\frac{1}{|r|}\right), \tag{36}$$

where T is the round trip travel time of a photon in the cavity, Eq. (24). Equation (36) tells us that by changing the reflection coefficient from $r=-0.99$ $(\ln(1/|r|)=10^{-2})$ to $r=-0.9999$ $(\ln(1/|r|)=10^{-4})$–a value which is well within the reach of contemporary experimental techniques [43], we reduce γ_c by two orders of magnitude.

The case of $r=-0.9999$ is illustrated graphically in Fig. 3(a) with other parameters being the same as in Fig. 2, which demonstrates that the strong coupling regime with reversible spontaneous decay is achievable when $m=1$. This is one of the main results of our paper. The Rabi oscillations have

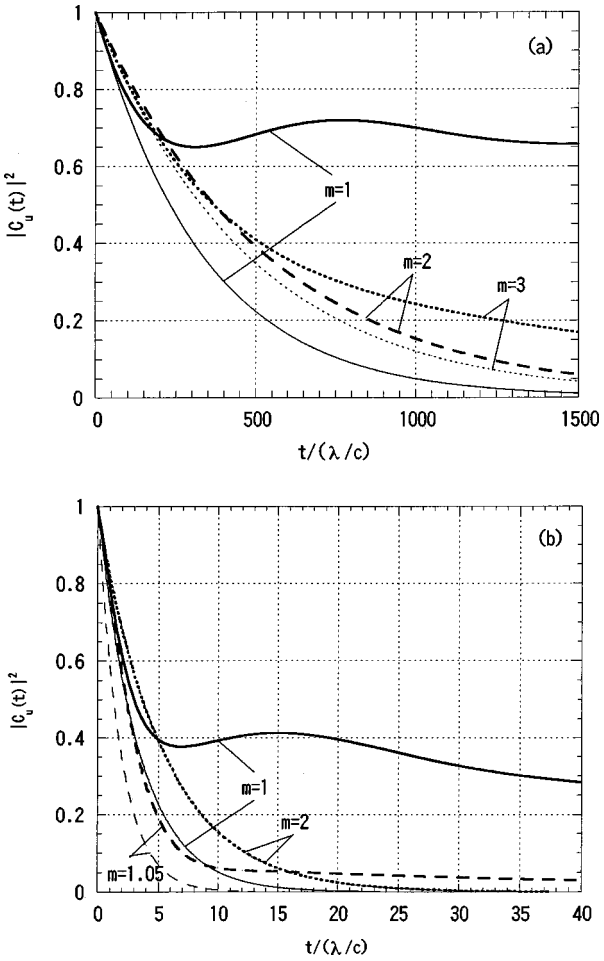

FIG. 3. Time evolution of the atomic upper-state population for different values of the scaled cavity length $m=l/(\lambda/2)$. Nonperturbative results are represented by bold curves and perturbative ones by light curves. The atom is placed at the cavity center and has its dipole oriented parallel to the mirror surfaces. Other parameters are (a) $A_0\lambda/(2c)=10^{-3}$ and $r=-0.9999$ and (b) $A_0\lambda/(2c)=10^{-1}$ and $r=-0.99$.

poor visibility and are rather fragile, though. They disappear, for instance, when the dipole is z-oriented or when the cavity length slightly increases. Several other values of m are also shown in Fig. 3(a). When $m=3$, although no oscillations are seen, there is still a large discrepancy between nonperturbative and perturbative results, while when $m=2$, the two are in good agreement. Vacuum-field Rabi splittings [44] and vacuum-field Rabi oscillations [45] in a Fabry-Perot cavity have been observed with two-dimensional quantum well excitons embedded in planar monolithic semiconductor structures (see [46] for more references.) There are some differences between the atomic decay process discussed here and the exciton decay experiments reported in [44–46]. For example, while the atom is coupled to all oblique modes, the excitons in a two-dimensional quantum well are coupled only to those with the same in-plane wave vectors as their own. The vacuum-field Rabi oscillations effects in the quantum well experiments have also been enhanced due to cooperative interaction [47]. Nevertheless, there is no doubt that the two cases are closely related and a study of one of them can shed light on the other [1].

To facilitate the strong coupling regime, in Fig. 3(a) we

have chosen to take a high cavity finesse. Alternatively, a large value of $A_0\lambda/(2c)$ can also be tried as is done in Fig. 3(b) with $A_0\lambda/(2c)=10^{-1}$, and as is expected, vacuum-field Rabi oscillations appear for $m=1$. When $m=2$, there is again a good agreement between the nonperturbative and perturbative theories, whereas when $m=1.05$, some discrepancy between the two can be noticed. This is due to the fact that, as will be shown below, the emission pattern in this case is better concentrated along the z-direction than in the case of $A_0\lambda/(2c)=10^{-3}$ presented in Fig. 2. Note that though the value $A_0\lambda/(2c)=10^{-1}$ is too high for a typical atomic optical transition, it can be achieved using excitons which may have a radiative lifetime of the order of a picosecond in GaAs quantum wells or even a subpicosecond in CdS quantum wells [48].

IV. SPONTANEOUS-EMISSION PATTERN

A. Observable field intensity

In order to calculate the observable field intensity, we start with the quantized mode expansions for the negative and positive parts of the electric field operator

$$\hat{\mathbf{E}}^{(+)}(\mathbf{r})=[\hat{\mathbf{E}}^{(-)}(\mathbf{r})]^{\dagger}=i\sum_j \sqrt{\frac{\hbar\omega_j}{2}}\mathbf{U}_j(\mathbf{r})\hat{a}_j, \tag{37}$$

and introduce the field state

$$|\gamma(t)\rangle=\sum_j C_{1j}(t)e^{-i\omega_j t}|\{1_j\}\rangle. \tag{38}$$

Then in terms of

$$\mathbf{F}(\mathbf{r},\mathbf{r}_{\mathrm{A}},t)=\langle 0|\hat{\mathbf{E}}^{(+)}(\mathbf{r})|\gamma(t)\rangle, \tag{39}$$

which can be interpreted as a kind of wave function for a photon, the observable field intensity at a position $\mathbf{r}_{\mathrm{B}}$ is

$$\begin{aligned} I(\mathbf{r}_{\mathrm{B}},\mathbf{r}_{\mathrm{A}},t)&\equiv\langle\psi(t)|\hat{\mathbf{E}}^{(-)}(\mathbf{r}_{\mathrm{B}})\hat{\mathbf{E}}^{(+)}(\mathbf{r}_{\mathrm{B}})|\psi(t)\rangle\\ &=\langle\gamma(t)|\hat{\mathbf{E}}^{(-)}(\mathbf{r}_{\mathrm{B}})\hat{\mathbf{E}}^{(+)}(\mathbf{r}_{\mathrm{B}})|\gamma(t)\rangle\\ &=|\mathbf{F}(\mathbf{r}_{\mathrm{B}},\mathbf{r}_{\mathrm{A}},t)|^2. \end{aligned} \tag{40}$$

Making use of Eqs. (37)–(39) and formally integrating Eq. (19), we rewrite $\mathbf{F}(\mathbf{r}_{\mathrm{B}},\mathbf{r}_{\mathrm{A}},t)$ in the form

$$\begin{aligned} \mathbf{F}(\mathbf{r}_{\mathrm{B}},\mathbf{r}_{\mathrm{A}},t)=ie^{-i\omega_{\mathrm{A}}t}\int_0^t dt' C_u(t')\sum_j \frac{\omega_j}{2}\mathbf{U}_j(\mathbf{r}_{\mathrm{B}})\\ \times[\mathbf{U}_j(\mathbf{r}_{\mathrm{A}})\cdot\boldsymbol{\mu}]e^{-i(\omega_j-\omega_{\mathrm{A}})(t-t')}. \end{aligned} \tag{41}$$

By inserting appropriate mode functions $\mathbf{U}_j(\mathbf{r}_{\mathrm{B}})$ in Eq. (41), after some tedious algebra (see Appendix C), we arrive at the following expression for the field observed from outside the cavity,

$$\begin{aligned} &F_{x,y,z}(\mathbf{r}_{\mathrm{B}},\mathbf{r}_{\mathrm{A}},t)\\ &=\frac{i\mu k_{\mathrm{A}}^3}{4\pi\epsilon_0}e^{-i\omega_{\mathrm{A}}t}\sum_{n=0}^{\infty}\sqrt{1-r^2}r^{2n}\\ &\times\left[f_{x,y,z}(R_{rn})e^{ik_{\mathrm{A}}R_{rn}}C_u\left(t-\frac{R_{rn}}{c}\right)H\left(t-\frac{R_{rn}}{c}\right)\right.\\ &\left.\pm rf_{x,y,z}(R_{\ln})e^{ik_{\mathrm{A}}R_{\ln}}C_u\left(t-\frac{R_{\ln}}{c}\right)H\left(t-\frac{R_{\ln}}{c}\right)\right], \end{aligned} \tag{42}$$

where

$$R_{rn}=[x_{\mathrm{B}}^2+y_{\mathrm{B}}^2+(z_{\mathrm{B}}-z_{\mathrm{A}}+2nl)^2]^{1/2}, \tag{43a}$$

$$R_{\ln}=\{x_{\mathrm{B}}^2+y_{\mathrm{B}}^2+[z_{\mathrm{B}}+z_{\mathrm{A}}+(2n+1)l]^2\}^{1/2}. \tag{43b}$$

The coefficient $f_{x,y,z}(R)$ with R being either R_{rn} or $R_{\ln}$ is given by, for a y-oriented dipole,

$$f_x^y(R)=-\frac{x_{\mathrm{B}}y_{\mathrm{B}}}{R^2}\left[\frac{1}{ik_{\mathrm{A}}R}+\frac{3}{(k_{\mathrm{A}}R)^2}-\frac{3}{i(k_{\mathrm{A}}R)^3}\right], \tag{44a}$$

$$f_y^y(R)=\frac{1}{ik_{\mathrm{A}}R}\left(1-\frac{y_{\mathrm{B}}^2}{R^2}\right)+\left[\frac{1}{(k_{\mathrm{A}}R)^2}-\frac{1}{i(k_{\mathrm{A}}R)^3}\right]\left(1-\frac{3y_{\mathrm{B}}^2}{R^2}\right), \tag{44b}$$

$$f_z^y(R)=-\frac{y_{\mathrm{B}}\sqrt{R^2-(x_{\mathrm{B}}^2+y_{\mathrm{B}}^2)}}{R^2}\left[\frac{1}{ik_{\mathrm{A}}R}+\frac{3}{(k_{\mathrm{A}}R)^2}-\frac{3}{i(k_{\mathrm{A}}R)^3}\right], \tag{44c}$$

and, for a z-oriented dipole,

$$f_x^{\perp}(R)=-\frac{x_{\mathrm{B}}\sqrt{R^2-(x_{\mathrm{B}}^2+y_{\mathrm{B}}^2)}}{R^2}\left[\frac{1}{ik_{\mathrm{A}}R}+\frac{3}{(k_{\mathrm{A}}R)^2}-\frac{3}{i(k_{\mathrm{A}}R)^3}\right], \tag{45a}$$

$$f_y^{\perp}(R)=-\frac{y_{\mathrm{B}}\sqrt{R^2-(x_{\mathrm{B}}^2+y_{\mathrm{B}}^2)}}{R^2}\left[\frac{1}{ik_{\mathrm{A}}R}+\frac{3}{(k_{\mathrm{A}}R)^2}-\frac{3}{i(k_{\mathrm{A}}R)^3}\right], \tag{45b}$$

$$\begin{aligned} f_z^{\perp}(R)=\frac{1}{ik_{\mathrm{A}}R}\frac{x_{\mathrm{B}}^2+y_{\mathrm{B}}^2}{R^2}+\left[\frac{1}{(k_{\mathrm{A}}R)^2}-\frac{1}{i(k_{\mathrm{A}}R)^3}\right]\\ \times\left[\frac{3(x_{\mathrm{B}}^2+y_{\mathrm{B}}^2)}{R^2}-2\right]. \end{aligned} \tag{45c}$$

In Eq. (42), the ''+''- and ''−''-signs are for y-oriented and z-oriented dipoles, respectively, and $C_u(t)$ is to be taken from Eqs. (22) or (28). Equations (42)–(45), together with Eq. (40), completely determine the field intensity observed from outside the cavity for an arbitrary space-time point and for both weak and strong coupling regimes. It can be verified that when the observing point is on the z-axis, our results are consistent with those given in [17] for the electric field operator in the Heisenberg picture.

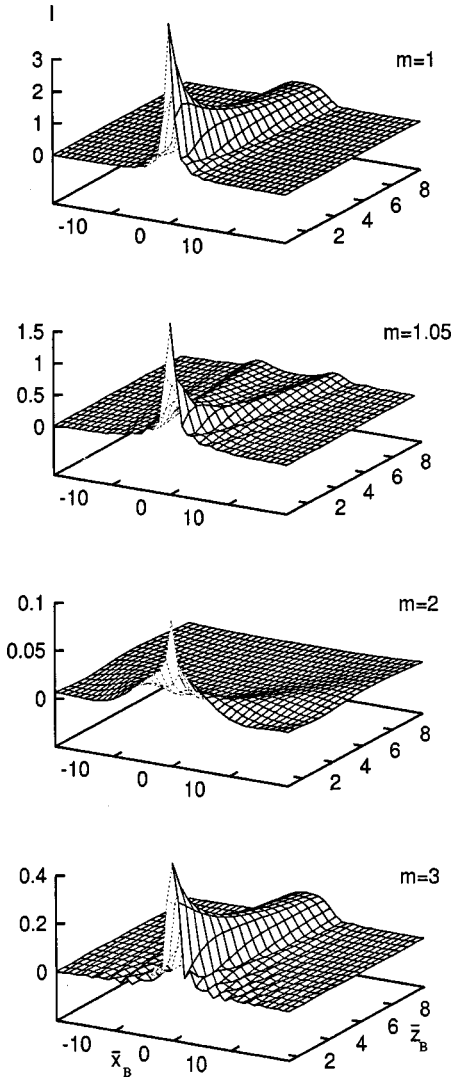

FIG. 4. Near-field emission pattern and its transition to far field for different values of the scaled cavity length m and for $A_0\lambda/(2c)=10^{-3}$, $r=-0.99$, and $\bar{t}\equiv t/(\lambda/c)=50$. The atom is at the cavity center with a y-oriented dipole and the observing point is outside the cavity with coordinates $(x_B,0,z_B)$. For brevity, we denote $\bar{x}_B\equiv x_B/(\lambda/2)$ and $\bar{z}_B\equiv z_B/(\lambda/2)$. The field intensity I is in the units of $10^{-5}[3c\hbar k_A^4/(16\pi^2\epsilon_0)]$.

B. Numerical results

1. From near field to far field

By near field and far field we mean the field near to and far away from the cavity mirror surfaces. We shall concentrate, as before, on a y-oriented dipole. Though in this case the field intensity varies in different manners when the observing point is moved along the x- and y-axis as can be seen from Eqs. (44), numerical calculations show that the emission pattern is almost symmetric about the z-axis.

An example of spontaneous emission pattern in the weak coupling regime is depicted in Fig. 4 for different values of the scaled cavity length $m=l/(\lambda/2)$ and for the time moment $\bar{t}\equiv t/(\lambda/c)=50$, with the atom being at the cavity center and with $A_0\lambda/(2c)=10^{-3}$ and $r=-0.99$, i.e., the same as in Fig. 2. The observation point lies within the xz-plane ($y_B=0$). We also denote, for brevity, $\bar{x}_B\equiv x_B/(\lambda/2)$ and $\bar{z}_B\equiv z_B/(\lambda/2)$ and start to increase $\bar{z}_B$ from $\bar{z}_B=m/2$–the value immediately at the right cavity wall. From the figure it can be seen that as a rule, the near-field emission pattern in the weak coupling regime consists of a single peak along the z-axis with some structures around it. These structures quite resemble the interference pattern in a Young's double-slit experiment, and indeed can be interpreted as resulting from the interference of a single photon with itself, or from the interference among the ''photons'' emitted by the original atom and its mirror images. When the cavity length increases, the near-field pattern tends to broaden and have a more complicated structure, though the broadening is less significant for odd m. In the case of $m=1.05$, though the spontaneous emission enhancement is larger than that in the case of $m=1$, the emission in the z-direction–the only direction in which the reflected light can act back on the atom, is lower, leading to a better performance of the perturbative theory as we have already mentioned.

At a distance of about several wavelengths from the cavity walls, the far-field emission pattern emerges and our results can be seen to be consistent with earlier perturbative calculations [15,16,18–20]. Namely, the far-field consists of a single pencil-like lobe pointed along the z-axis when $m=1$ and is split up into a conical shape when the cavity is slightly longer than half wavelength ($m=1.05$ in our case). Such patterns have been experimentally observed [18]. When the cavity gap is one wavelength ($m=2$), the far-field pattern is also of a conical shape, which covers a larger solid angle and is more spread than that in the case of $m=1.05$. When $m=3$, though perturbative theory predicts a central lobe and a conical lobe [16], the conical lobe is too weak to be visible in the plot.

With parameters $A_0\lambda/(2c)=10^{-3}$ and $r=-0.99$ considered in Fig. 4, the distance from the cavity walls required for the far-field pattern to be fully established, when translated into time, is very small as compared to the atomic and cavity decay times. We therefore may assume a quasi-steady state, in which the near and far field are related through a Fourier transform according to the diffraction theory [49]. Take, for instance, the cases of $m=1$ and $m=3$. The diffraction theory tells us that the diffraction pattern of a circular aperture is a so-called Airy's pattern with a central disk and multiple rings around it [49]. In our case, for a circular single lobe to appear in the far field, there must be an equivalence of the Airy's pattern in the near field, and as can be seen from Fig. 4, that is indeed the case.

Another situation of interest when $A_0\lambda/(2c)=10^{-1}$, i.e., when the atomic natural decay is very fast, is presented in Fig. 5. When the cavity gap is one half wavelength ($m=1$), the emission pattern is in overall similar to that in the weak coupling regime shown in Fig. 3, except that now the spontaneous emission pulse has a much higher intensity. When $m=1.05$, there is however, a significant change in the behavior of the far field: the emission pattern, though spreads as z_B increases, does not split into a conical shape as in the weak coupling regime. When $m=2$ the near-field pattern may become quite complicated while the far-field pattern still can be treated as of a conical shape. When $m=3$, beside the central lobe, we see that a weaker conical lobe is also present [16]. Our numerical results for earlier times and the cases of $m=2$ and $m=3$ in Fig. 5 demonstrate that the emis-

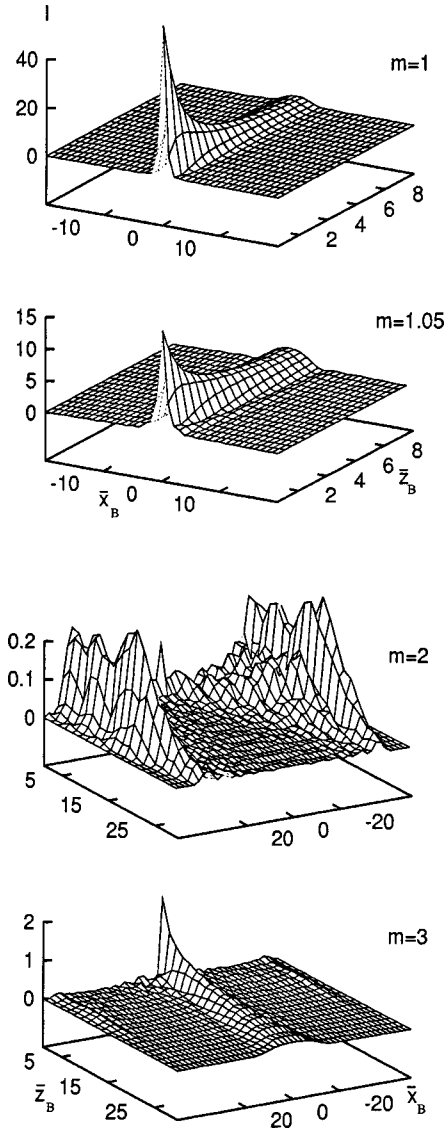

FIG. 5. Near-field emission pattern and its transition to far field for different values of the scaled cavity length m and for $A_0\lambda/(2c)=10^{-1}$, $r=-0.99$, and $\bar{t}=25$. The atom is at the cavity center with a y-oriented dipole and the observing point is outside the cavity with coordinates $(z_B,0,z_B)$. For brevity, we denote $\bar{z}_B \equiv x_B/(\lambda/2)$ and $\bar{z}_B \equiv z_B/(\lambda/2)$. The field intensity I is in the units of $10^{-5}[3c\hbar k_A^4/(16\pi^2\epsilon_0)]$.

sion pattern exhibits a more kinky behavior than in the case presented in Fig. 4. The reason is that these kinks are caused by the arrival of the reflected radiations, each of which has a greater impact on the atom in a fast decay process than in a slower one.

2. Effective mode radius and near-field pattern

The Fabry-Perot cavity has a peculiar feature that in spite of its infinite lateral extent, the cavity mode volume is finite with an effective mode radius [15,31]

$$r_{\mathrm{eff}}=\sqrt{\frac{\pi l\lambda|r|}{8(1-r^2)}}. \tag{46}$$

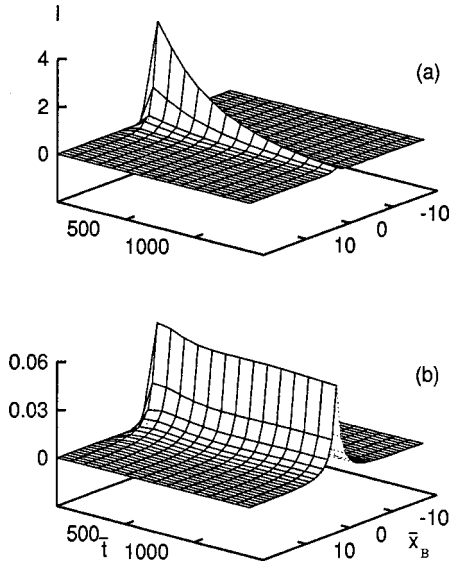

FIG. 6. Time evolution of the near-field emission pattern ($\bar{z}_B = m/2$) for (a) $r=-0.99$ and (b) $r=-0.9999$. Other parameters are the same as in Fig. 4.

This effective mode radius determines the distance over which two microlasers sharing the same Fabry-Perot cavity are correlated and is also called the transverse quantum correlation length [30]. Such transverse quantum correlation and effective mode radius have been observed experimentally [30,50]. The near-field pattern, clearly, can be taken as yet another indicator of the finite effective mode volume. When $r=-0.99$, Eq. (46) yields an effective mode radius of $r_{\mathrm{eff}}/(\lambda/2)\sim 6\sqrt{m}$, in very good agreement with the near-field pattern shown in Fig. 4. Thus, an excited atom enclosed in a Fabry-Perot cavity, when looked at from outside, behaves not as a point-like emitting source, but as an emitting spot with finite size which is defined by Eq. (46), and which can be many times larger than the wavelength.

Since the spontaneous decay is a transient process, a question may arise about whether the near-field emission pattern spreads in time. This question is addressed in Fig. 6(a), where we depict the time evolution of the near-field pattern right at the cavity wall ($\bar{z}_B=m/2$) for $A_0\lambda/(2c)=10^{-3}$, $r=-0.99$, and $m=1$. It can be seen that the spread is not significant, that is, the consistency between the effective mode radius and the near-field pattern is preserved. Another point is the dependence of the effective mode radius on the mirrors reflectivity. According to Eq. (46), r_{eff} increases with an increasing $|r|$, and the use of an ideal cavity with infinite finesse leads to a single plane-wave structure for the longitudinal mode, and to infinite transverse extent of that mode. In particular, for $r=-0.9999$, we have $r_{\mathrm{eff}}\sim 60\sqrt{m}$, i.e., a spread in the near-field pattern ten times larger than that for $r=-0.99$ is expected. Numerical results presented in Fig. 6(b) where the time evolution of the near field for $A_0\lambda/(2c)=10^{-3}$, $r=-0.9999$, and $m=1$ is plotted, however, show that the spread is almost the same as in the case of $r=-0.99$. This can be explained as follows. In deriving Eq. (46), a weak coupling regime has been assumed in which once the photon is emitted, it will smear over the transverse extension of the mode. An increase in the mirrors reflectivity, however, as we have shown in Section III, may give rise

to a strong coupling regime, in which the initially emitted photon can be repeatedly re-absorbed and re-emitted. These multiple re-absorptions and re-emissions, in turn, result in a good localization of the photon near the atomic position. Since the transverse mode size identifies the minimum transverse size required for a microcavity laser of planar type even if the pumped region is smaller, the fact that the transverse mode size does not increase with an increasing mirror reflectivity as much as Eq. (46) predicts may be beneficial in designing optical integrated systems in which very small size of a single component is desirable [1].

Now let us come back to the direct comparison of the three coupling constants κ, γ_c, and γ'. Recall that we are interested in the case where the atom is at the cavity center, its dipole is *y*-oriented and the cavity gap is of one half wavelength ($m=1$). Hence it is reasonable to assume that [1,20]

$$\gamma' \ll A_0 . \tag{47}$$

To estimate κ, we assume that the emission occurs into the effective volume of the longitudinal cavity mode $V_{\rm eff} = l\pi r_{\rm eff}^2$ and that the emission rate in the cavity is of the same order as the free-space rate [20]. Then we can replace $\mathbf{U}_j(\mathbf{r}_A)$ in Eq. (16) by $2/\sqrt{\epsilon_0 V_{\rm eff}}$ to have

$$\kappa = \left(\frac{6\pi c^3 A_0}{V_{\rm eff}\omega_A^2} \right)^{1/2} . \tag{48}$$

We shall take $\lambda = 10^{-6} m$. (i) $r=-0.99$ and $A_0\lambda/(2c) = 10^{-3}$. Eqs. (36) and (46)–(48) give us $\gamma_c \sim 10^{12}\,{\rm s}^{-1}$, $\gamma' \ll 10^{11}\,{\rm s}^{-1}$, and $\kappa \sim 10^{12}\,{\rm s}^{-1}$. Since $\kappa \sim \gamma_c$, we have a weak coupling regime as is seen in Fig. 2. (ii) $r=-0.9999$ and $A_0\lambda/(2c)=10^{-3}$. Eqs. (36) and (46)–(48) lead to $\gamma_c \sim 10^{10}\,{\rm s}^{-1}$, $\gamma' \ll 10^{11}\,{\rm s}^{-1}$, and $\kappa \sim 10^{12}\,{\rm s}^{-1}$, i.e., $\kappa \gg \gamma_c, \gamma'$. This means a strong coupling regime, in agreement with the numerical results presented in Fig. 3(a). (iii) $r=-0.99$ and $A_0\lambda/(2c)=10^{-1}$. Hence we have $\gamma_c \sim 10^{12}\,{\rm s}^{-1}$, $\gamma' \ll 10^{13}\,{\rm s}^{-1}$, and $\kappa \sim 10^{13}\,{\rm s}^{-1}$, i.e., $\kappa \gg \gamma_c, \gamma'$ and a strong coupling regime follows, in agreement with Fig. 3(b). It is worth noting that we have used the formula (46) to evaluate $r_{\rm eff}$ in all three estimations above. If we use a reduced effective mode radius consistent with our results on the near-field pattern, the relationship $\kappa \gg \gamma_c, \gamma'$ in cases (ii) and (iii) will be improved even further.

V. CONCLUSIONS

We have used a three-dimensional nonperturbative approach to study spontaneous emission in a Fabry-Perot cavity based on a complete set of orthogonal standing-wave mode functions. In the weak coupling regime where Fermi's golden rule holds, it has been shown that these mode functions reproduce exactly the same spontaneous-emission rate as that derived using traveling-wave modes. We have obtained a general delay-differential equation for the probability amplitude of the initially excited state, which can be employed to study the effects of the cavity length, cavity mirrors reflectivity, atomic position and dipole orientation, etc., on the spontaneous decay process. The delay terms in this equation can be associated with the back action of the emitted light on the atom after successive reflections at the cavity walls. Such retarded interaction is absent in a nonperturbative theory which is based on a single-mode description of the electromagnetic field. Further, analytic solution to the delay-differential equation has been obtained for the special case when the atom is positioned at the cavity center. This solution and the original delay-differential equation have been used to investigate numerically the time behavior of the atomic state populations. Our results are then compared with perturbative ones. We have found that even though the Fabry-Perot cavity has space confinement in only one direction, strong coupling regime and together with it vacuum-field Rabi oscillations are still possible. Conditions favorable for this strong coupling regime include a half wavelength cavity, a dipole placed at an antinode position and oriented parallel to the mirror surfaces, a high enough cavity finesse or a large enough dipole matrix element.

Next, we have derived a general expression for the field intensity observed from outside the cavity which holds for an arbitrary space-time point and atom-radiation coupling strength and used it to study numerically the spontaneous-emission pattern in both weak and strong coupling regimes. The far-field pattern in the weak coupling regime has been shown to be consistent with previously known perturbative results. We have found that for a moderate value of the mirror reflection coefficient, the broadening in the near-field pattern is in good agreement with the concept of effective mode radius. As the mirror reflectivity increases, however, because of the strong-coupling the photon is better localized than is predicted by the effective mode concept. We suggest that this can be verified experimentally using the same setup as, e.g., in [44] where time-resolved vacuum Rabi oscillations have been observed.

The planar cavity used in our treatment is an idealized cavity with lossless and infinitely thin mirrors which have wavelength and incident angle independent reflectivity. Lossless and highly reflecting mirrors used in reality are Bragg mirrors made by stacking pairs of dielectric layers, one with high index of refraction and another with low index of refraction. Such mirrors have finite thickness and nonuniform reflectivity. Nevertheless, it is reasonable to assume that qualitatively, effects predicted by an ideal-cavity theory will persist under realistic and appropriate conditions. In fact, many of them have actually been observed. For example, the existence of an effective mode radius has been experimentally verified in the weak coupling regime by investigating interatom quantum correlations established between two equal localized sets of excited dye molecules placed in two spots in the microcavity [30] and by studying the probability distributions in the intensity of two pulsed planar microcavity dye lasers, one with single-mode operation and another with multimode operation [50] and the vacuum-field Rabi oscillations and vacuum-field Rabi splitting have been observed with exciton-photon interaction in semiconductor microcavities [44–46], as we have mentioned earlier. The assumption on the infinitely far extension of the mirrors in the *xy* plane is not severe. If the transverse size of the cavity is larger than the effective mode radius, which can be calculated using Eq. (46) in the weak coupling regime or estimated through the near-field pattern in the strong coupling regime, we expect that the main physical results of this

work will not be affected in any substantial way.

Another potentially useful property of spontaneous emission in a microcavity is the spectral line narrowing. Due to a reduction of the number of allowed photon modes, light can have a spectrum much narrower than that in the ordinary free-space emission. The spectrum of spontaneous emission in a one-dimensional monolayer optical cavity has been calculated in [27], and the formalism developed there can be adapted easily to our case. Work on the spectral properties of spontaneous emission in a Fabry-Perot microcavity is in progress and the results will be reported elsewhere.

ACKNOWLEDGMENTS

We thank Professor H. Hairer for providing us with the FORTRAN code for solving a system of first-order delay-differential equations, and G. Nakayama for helping with the computer plots. H.T.D. gratefully acknowledges financial support from the Nishina Memorial Foundation and thanks the University of Electro-Communications for hospitality.

APPENDIX A: EVALUATION OF THE KERNEL $K(t-t')$

In order to evaluate the kernel $K(t-t')$, Eq. (21), we replace the summation over the mode index j by an integral over k, θ, and ϕ as

$$\sum_j \rightarrow \sum_c \frac{V}{(2\pi)^3}\int_0^{\pi} d\phi \int_0^{\pi/2} d\theta \sin\theta \int_0^{\infty} dk\, k^2, \quad \text{(A1)}$$

where Σ_c denotes the sum over the mode categories. The components of the **k**-vector are

$$k_x = k\sin\theta\cos\phi, \quad k_y = k\sin\theta\sin\phi, \qquad k_p = k\sin\theta, \quad k_z = k\cos\theta \quad \text{(A2)}$$

with θ being the angle between **k** and the z-axis and ϕ being the angle between $\mathbf{k}_p$ and the x-axis. Note that the upper limits of integrations over θ and ϕ are $\pi/2$ and π, respectively, because we are using standing-wave mode functions rather than traveling-wave mode functions.

Let us consider first the case of a dipole oriented parallel to the cavity mirror surfaces. To be definite, let it be a y-oriented dipole. Using Eqs. (21), (16), (A1), and the mode functions given in Section II, the sum over the categories of modes yields (only even-x-y modes contribute since $\sin(\mathbf{k}_p \cdot \mathbf{r}_A) = 0$)

$$\begin{aligned} K(t-t') &= -\frac{V}{(2\pi)^3}\int_0^{\pi} d\phi \int_0^{\pi/2} d\theta \sin\theta \\ &\quad \times \int_0^{\infty} dk\, k^2 \frac{ck}{2\hbar} e^{-ic(k-k_A)(t-t')} \sum_c |\mathbf{U}(\mathbf{r}_A)\cdot\boldsymbol{\mu}|^2 \\ &= -\frac{V}{(2\pi)^3}\int_0^{\pi} d\phi \int_0^{\pi/2} d\theta \sin\theta \\ &\quad \int_0^{\infty} dk \frac{ck^3}{2\hbar} e^{-ic(k-k_A)(t-t')} \\ &\quad \times \frac{4\mu^2}{\epsilon_0 V}(\cos^2\phi + \sin^2\phi\cos^2\theta) \\ &\quad \times \Bigg(1 + 2\sum_{n=1}^{\infty} r^{2n}\cos(k\cos(\theta)2nl) \\ &\quad + \sum_{n=0}^{\infty} r^{2n+1}\{\cos[k\cos(\theta)((2n+1)l+2z_A)] \\ &\quad + \cos[k\cos(\theta)((2n+1)l-2z_A)]\}\Bigg). \end{aligned} \quad \text{(A3)}$$

After taking the integration over the angle variables we get

$$\begin{aligned} K(t-t') &= -\frac{\mu^2 c}{2\pi^2\hbar\epsilon_0}\int_0^{\infty} dk\, k^3 e^{-ic(k-k_A)(t-t')} \\ &\quad \times \Bigg(\frac{1}{3} + \sum_{n=1}^{\infty} r^{2n} g(k2nl) \\ &\quad + \frac{1}{2}\sum_{n=0}^{\infty} r^{2n+1}(g\{k[(2n+1)l+2z_A]\} \\ &\quad + g\{k[(2n+1)l-2z_A]\})\Bigg), \end{aligned} \quad \text{(A4)}$$

where

$$g(x) = \frac{\sin x}{x} + \frac{\cos x}{x^2} - \frac{\sin x}{x^3}. \quad \text{(A5)}$$

The integral over k can now be performed, e.g., as

$$\begin{aligned} &\int_0^{\infty} dk\, k^3 e^{-ic(k-k_A)(t-t')}\frac{\sin k2nl}{k2nl} \\ &= \int_0^{\infty} dk \frac{k^2}{2nl}\frac{1}{2i}[e^{-ic(k-k_A)(t-t'-2nl/c)}e^{ik_A 2nl} \\ &\quad - e^{-ic(k-k_A)(t-t'+2nl/c)}e^{-ik_A 2nl}] \\ &= \int_{-\infty}^{\infty} dy \frac{(k_A+y)^2}{2nl}\frac{1}{2i}[e^{-icy(t-t'-2nl/c)}e^{ik_A 2nl} \\ &\quad - e^{-icy(t-t'+2nl/c)}e^{-ik_A 2nl}] \\ &= \frac{\pi k_A^2}{ic2nl}[\delta(t-t'-2nl/c)e^{ik_A 2nl} \\ &\quad - \delta(t-t'+2nl/c)e^{-ik_A 2nl}], \end{aligned} \quad \text{(A6)}$$

where in going from the first equation to the second we have set $(k-k_A)\rightarrow y$ and replaced the lower limit of the integral $-k_A$ by $-\infty$, as is usually done in a standard Weisskopf-Wigner theory. We have further retained the dependence on y only in the exponential by assuming that the time variation

of $C_u(t)$ is slow as compared to the atomic oscillations at the optical frequency. Similar approximation has also been used in [23–25,38]. Other terms on the right hand side of Eq. (A4) can be dealt with in the same manner and we finally have

$$K(t-t')=A_0\Bigg(\delta(t-t')+\frac{3}{2}\sum_{n=1}^{\infty}r^{2n}h(2nl)+\frac{3}{4}\sum_{n=0}^{\infty}r^{2n+1}\{h[(2n+1)l+2z_A]+h[(2n+1)l-2z_A]\}\Bigg), \tag{A7}$$

where

$$h(x)=\frac{1}{ik_Ax}[\delta(t-t'-x/c)e^{ik_Ax}-\delta(t-t'+x/c)e^{-ik_Ax}]+\frac{1}{(k_Ax)^2}[\delta(t-t'-x/c)e^{ik_Ax}+\delta(t-t'+x/c)e^{-ik_Ax}]-\frac{1}{i(k_Ax)^3}[\delta(t-t'-x/c)e^{ik_Ax}+\delta(t-t'+x/c)e^{-ik_Ax}], \tag{A8}$$

and A_0 is the free-space spontaneous decay rate given in Eq. (23). Substituting Eqs. (A7) and (A8) in Eq. (20), we obtain readily the delay-differential equation (22). The case when the dipole is oriented perpendicular to the cavity mirror surfaces can be dealt with in the same way as outlined above.

APPENDIX B: PROOF OF EQ. (28)

By introducing the notation

$$\tilde{C}_u(t)\equiv C_u(t)\exp\left(\frac{A_0}{2}t\right),\quad \tilde{p}_n\equiv p_n(k_Anl)\exp\left(\frac{A_0}{2}\frac{nl}{c}\right), \tag{B1}$$

equation (26) can be simplified further

$$\dot{\tilde{C}}_u(t)=\sum_{n=1}^{\infty}\tilde{p}_n\tilde{C}_u(t_n)H(t_n). \tag{B2}$$

For times $t\leqslant l/c$, Eq. (B2) becomes an ordinary differential equation which can be integrated easily. Once the solution for $t\leqslant l/c$ is known, we can integrate the equation for $l/c\leqslant t\leqslant 2l/c$, and so on (for a discussion on the nature of the delay-differential equations, see [51].) The results of several first steps are, with the initial condition of $\tilde{C}_u(0)=1$,

$$\tilde{C}_u(t)=1 \text{ for } 0\leqslant t\leqslant l/c,$$

$$\tilde{C}_u(t)=1+\tilde{p}_1t_1 \text{ for } l/c\leqslant t\leqslant 2l/c,$$

$$\tilde{C}_u(t)=1+\tilde{p}_1t_1+\tilde{p}_1^2\frac{t_2^2}{2!}+\tilde{p}_2t_2 \text{ for } 2l/c\leqslant t\leqslant 3l/c,$$

$$\tilde{C}_u(t)=1+\tilde{p}_1t_1+\tilde{p}_1^2\frac{t_2^2}{2!}+\tilde{p}_2t_2+\tilde{p}_1^3\frac{t_3^3}{3!}+2\tilde{p}_1\tilde{p}_2\frac{t_3^2}{2!}+\tilde{p}_3t_3 \text{ for } 3l/c\leqslant t\leqslant 4l/c,$$

$$\tilde{C}_u(t)=1+\tilde{p}_1t_1+\tilde{p}_1^2\frac{t_2^2}{2!}+\tilde{p}_2t_2+\tilde{p}_1^3\frac{t_3^3}{3!}+2\tilde{p}_1\tilde{p}_2\frac{t_3^2}{2!}+\tilde{p}_3t_3+\tilde{p}_1^4\frac{t_4^4}{4!}+3\tilde{p}_1^2\tilde{p}_2\frac{t_4^3}{3!}+2\tilde{p}_1\tilde{p}_3\frac{t_4^2}{2!}+\tilde{p}_2^2\frac{t_4^2}{2!}+\tilde{p}_4t_4 \text{ for } 4l/c\leqslant t\leqslant 5l/c,$$

$$\ldots. \tag{B3}$$

From Eqs. (B3), it can be deduced that the solution of the delay-differential equation (B2) is of the form

$$\tilde{C}_{un}(t)=\sum_{k=0}^{n}\left(\sum\frac{m!}{a_1!a_2!\cdots a_k!}\tilde{p}_1^{a_1}\tilde{p}_2^{a_2}\cdots\tilde{p}_k^{a_k}\frac{t_k^m}{m!}\right) \text{ for } nl/c\leqslant t\leqslant(n+1)l/c \quad (n=0,1,2,\ldots), \tag{B4}$$

where the inner sum is over non-negative integers $a_i(i=1,2,\ldots,k)$ such that

$$1a_1+2a_2+\cdots+ka_k=k, \tag{B5}$$

and

$$m=a_1+a_2+\cdots+a_k. \tag{B6}$$

To prove that Eq. (B4) is indeed a solution of Eq. (B2), we differentiate both sides of it and use the recurrence formula

$$\frac{m!}{a_1!a_2!\cdots a_k!}=\frac{(m-1)!}{(a_1-1)!a_2!\cdots a_k!}+\frac{(m-1)!}{a_1!(a_2-1)!a_3!\cdots a_k!}+\cdots+\frac{(m-1)!}{a_1!a_2!\cdots a_{k-1}!(a_k-1)!} \tag{B7}$$

to obtain

$$
\begin{aligned}
\dot{\tilde{C}}_{un}(t) &= \sum_{k=1}^{n} \tilde{p}_1 \left[\sum \frac{(m-1)!}{(a_1-1)!a_2!\cdots a_k!} \tilde{p}_1^{a_1-1}\tilde{p}_2^{a_2}\cdots\tilde{p}_k^{a_k} \frac{t_k^{m-1}}{(m-1)!} \right] \\
&\quad + \sum_{k=2}^{n} \tilde{p}_2 \left[\sum \frac{(m-1)!}{a_1!(a_2-1)!\cdots a_k!} \tilde{p}_1^{a_1}\tilde{p}_2^{a_2-1}\cdots\tilde{p}_k^{a_k} \frac{t_k^{m-1}}{(m-1)!} \right] \\
&\quad \vdots \\
&\quad + \sum_{k=n}^{n} \tilde{p}_k \left[\sum \frac{(m-1)!}{a_1!a_2!\cdots(a_k-1)!} \tilde{p}_1^{a_1}\tilde{p}_2^{a_2}\cdots\tilde{p}_k^{a_k-1} \frac{t_k^{m-1}}{(m-1)!} \right] \\
&= \tilde{p}_1 \sum_{k=0}^{n-1} \left(\sum \frac{m!}{a_1!a_2!\ldots a_k!} \tilde{p}_1^{a_1}\tilde{p}_2^{a_2}\cdots\tilde{p}_k^{a_k} \frac{t_{k+1}^{m}}{m!} \right) \\
&\quad + \tilde{p}_2 \sum_{k=0}^{n-2} \left(\sum \frac{m!}{a_1!a_2!\cdots a_k!} \tilde{p}_1^{a_1}\tilde{p}_2^{a_2}\cdots\tilde{p}_k^{a_k} \frac{t_{k+2}^{m}}{m!} \right) \\
&\quad \vdots \\
&\quad + \tilde{p}_n \\
&= \tilde{p}_1 \tilde{C}_{u(n-1)}(t_1) + \tilde{p}_2 \tilde{C}_{u(n-2)}(t_2) + \cdots + \tilde{p}_n \tilde{C}_{u0}(t_n).
\end{aligned} \tag{B8}
$$

The lower limit of the outer sum in, for instance, the first term in the first equation, is 1 because this term will appear only if $a_1 \geqslant 1$, see Eq. (B7), which in turn means $k \geqslant 1$ in accordance with Eq. (B5). In going from the second equation to the last we have again made use of the solution (B4). The last equation is nothing else rather than Eq. (B2) and our proof is completed. The piecewise solution (B4) can be combined and transformed using (B1) to arrive at the solution (28).

APPENDIX C: PROOF OF EQS. (42)–(45)

Let us consider first the case of a *y*-oriented dipole. By replacing the sum over the modes in Eq. (41) by an integral as in Eq. (A1) we obtain

$$
\begin{aligned}
\mathbf{F}(\mathbf{r}_B,\mathbf{r}_A,t) &= \frac{iV}{(2\pi)^3} e^{-i\omega_A t} \int_0^t dt' C_u(t') \int_0^{\pi} d\phi \int_0^{\pi/2} d\theta \sin\theta \int_0^{\infty} dk\, k^2 \frac{ck}{2} e^{-ic(k-k_A)(t-t')} \sum_c \mathbf{U}(\mathbf{r}_B)[\mathbf{U}(\mathbf{r}_A)\cdot\boldsymbol{\mu}] \\
&= \frac{iV\mu}{(2\pi)^3} e^{-i\omega_A t} \int_0^t dt' C_u(t') \int_0^{\pi} d\phi \int_0^{\pi/2} d\theta \sin\theta \int_0^{\infty} dk \frac{ck^3}{2} e^{-ic(k-k_A)(t-t')} \Bigg\{ \hat{\mathbf{x}} \cos(\mathbf{k}_p\cdot\mathbf{r}_B) k_x k_y \\
&\quad \times \Bigg[-(\alpha^{ozTE})^2 \sin k_{1z} z_A u_0^{ozTE}(z_B) - (\alpha^{ezTE})^2 \cos k_{1z} z_A u_0^{ezTE}(z_B) - (\alpha^{ezTM})^2 k_{1z} \sin k_{1z} z_A \frac{d}{dz} u_0^{ezTM}(z) \Big|_{z_B} \\
&\quad + (\alpha^{ozTM})^2 k_{1z} \cos k_{1z} z_A \frac{d}{dz} u_0^{ozTM}(z) \Big|_{z_B} \Bigg] + \hat{\mathbf{y}} \cos(\mathbf{k}_p\cdot\mathbf{r}_B) \Bigg[(\alpha^{ozTE})^2 k_x^2 \sin k_{1z} z_A u_0^{ozTE}(z_B) \\
&\quad + (\alpha^{ezTE})^2 k_x^2 \cos k_{1z} z_A u_0^{ezTE}(z_B) + (\alpha^{ezTM})^2 k_y^2 (-k_{1z}) \sin k_{1z} z_A \frac{d}{dz} u_0^{ezTM}(z) \Big|_{z_B} \\
&\quad + (\alpha^{ozTM})^2 k_y^2 k_{1z} \cos k_{1z} z_A \frac{d}{dz} u_0^{ozTM}(z) \Big|_{z_B} \Bigg] + \hat{\mathbf{z}} \sin(\mathbf{k}_p\cdot\mathbf{r}_B) k_p^2 k_y k_{1z} [-(\alpha^{ezTM})^2 \sin k_{1z} z_A u_0^{ezTM}(z_B) \\
&\quad + (\alpha^{ozTM})^2 \cos k_{1z} z_A u_0^{ozTM}(z_B)] \Bigg\}.
\end{aligned} \tag{C1}
$$

Next we rewrite $u_0^{ozTE}(z)$, Eq. (2b), as

$$u_0^{\mathrm{ozTE}}(z)=\sqrt{\frac{k_{1z}}{k_{0z}}}\frac{k_{1z}+k_{0z}}{2\sqrt{k_{1z}k_{0z}}}\left\{\sin\left[k_{0z}\left(z-\frac{l}{2}\right)+k_{1z}\frac{l}{2}\right]+\frac{k_{1z}-k_{0z}}{k_{1z}+k_{0z}}\sin\left[k_{0z}\left(z-\frac{l}{2}\right)-k_{1z}\frac{l}{2}\right]\right\}$$

$$=\sqrt{\frac{k_{1z}}{k_{0z}}}\frac{1}{\sqrt{1-r^2}}\left\{\sin\left[k_{0z}\left(z-\frac{l}{2}\right)+k_{1z}\frac{l}{2}\right]+r\sin\left[k_{0z}\left(z-\frac{l}{2}\right)-k_{1z}\frac{l}{2}\right]\right\} \tag{C2}$$

with r defined as in Eq. (12). Clearly, similar expressions hold for other $u_0(z)$. After carrying out the same limiting procedure as discussed below Eq. (14), we get

$$\mathbf{F}(\mathbf{r}_\mathrm{B},\mathbf{r}_\mathrm{A},t)=\frac{iV\mu}{(2\pi)^3}e^{-i\omega_\mathrm{A}t}\int_0^t dt'\,C_u(t')\int_0^\infty dk\,\frac{ck^3}{2}e^{-ic(k-k_\mathrm{A})(t-t')}\int_0^{\pi/2}d\theta\sin\theta\int_0^\pi d\phi\frac{4}{\epsilon_0 V}\Bigg(\hat{\mathbf{x}}\cos(\mathbf{k}_p\cdot\mathbf{r}_\mathrm{B})\sin\phi\cos\phi$$

$$\times(-\sin^2\theta)\sum_{n=0}^{\infty}\sqrt{1-r^2}r^{2n}\{\cos[k_z(z_\mathrm{A}-z_\mathrm{B}-2nl)]+r\cos[k_z(z_\mathrm{A}+z_\mathrm{B}+(2n+1)l)]\}+\hat{\mathbf{y}}\cos(\mathbf{k}_p\cdot\mathbf{r}_\mathrm{B})$$

$$\times(\cos^2\phi+\sin^2\phi\cos^2\theta)\sum_{n=0}^{\infty}\sqrt{1-r^2}r^{2n}\{\cos[k_z(z_\mathrm{A}-z_\mathrm{B}-2nl)]+r\cos[k_z(z_\mathrm{A}+z_\mathrm{B}+(2n+1)l)]\}$$

$$+\hat{\mathbf{z}}\sin(\mathbf{k}_p\cdot\mathbf{r}_\mathrm{B})\sin\phi\sin\theta\cos\theta\sum_{n=0}^{\infty}\sqrt{1-r^2}r^{2n}\{\sin[k_z(z_\mathrm{A}-z_\mathrm{B}-2nl)]+r\sin[k_z(z_\mathrm{A}+z_\mathrm{B}+(2n+1)l)]\}\Bigg). \tag{C3}$$

Let's examine, for instance, the y-component. It contains the integrals over the angle variables

$$Z=\int_0^{\pi/2}d\theta\sin\theta\int_0^\pi d\phi\cos(\mathbf{k}_p\cdot\mathbf{r}_\mathrm{B})(\cos^2\phi+\sin^2\phi\cos^2\theta)\cos(c\cos\theta), \tag{C4}$$

where c can be either c_r or c_l

$$c_\mathrm{r}=k(z_\mathrm{B}-z_\mathrm{A}+2nl), \tag{C5a}$$

$$c_\mathrm{l}=k[z_\mathrm{B}+z_\mathrm{A}+(2n+1)l]. \tag{C5b}$$

The integration over ϕ can be dealt with as follows

$$\int_0^\pi d\phi\cos(\mathbf{k}_p\cdot\mathbf{r}_\mathrm{B})=\int_0^\pi d\phi\cos(k\sin\theta\cos\phi x_\mathrm{B}+k\sin\theta\sin\phi\ \ y_\mathrm{B})$$

$$=\int_0^\pi d\phi\cos[d\sin\theta\sin(\phi+\psi)]$$

$$=\int_\psi^{\pi+\psi}d\phi\cos(d\sin\theta\sin\phi)$$

$$=\int_0^\pi d\phi\cos(d\sin\theta\sin\phi)$$

$$=\pi J_0(d\sin\theta), \tag{C6}$$

where $J_0(x)$ is a Bessel function [52] and

$$d=k\sqrt{x_\mathrm{B}^2+y_\mathrm{B}^2},\quad \tan\psi=\frac{x_\mathrm{B}}{y_\mathrm{B}}. \tag{C7}$$

Here, we have made use of the fact that the integrand is a periodic function with period π, so that the integral limits can be shifted by an arbitrary amount, which is ψ in our case. Similarly, we find

$$\int_0^\pi d\phi\cos(\mathbf{k}_p\cdot\mathbf{r}_\mathrm{B})\cos 2\phi=\pi\cos(2\psi)J_2(d\sin\theta). \tag{C8}$$

Substituting (C6) and (C8) in Eq. (C4) gives

$$
\begin{aligned}
Z &= \frac{\pi}{2}\int_0^{\pi/2} d\theta \sin\theta[(1+\cos^2\theta)J_0(d\sin\theta)+(1-\cos^2\theta)\cos(2\psi)J_2(d\sin\theta)]\cos(c\cos\theta) \\
&= \pi\int_0^{\pi/2} d\theta \sin\theta\left[J_0(d\sin\theta)-\frac{\sin\theta}{d}J_1(d\sin\theta)+(\cos^2\psi)(\sin^2\theta)J_2(d\sin\theta)\right]\cos(c\cos\theta) \\
&= \pi\int_0^{\pi/2} d\theta \sin\theta\left[J_0(d\sin\theta)-\frac{\sin\theta}{d}J_1(d\sin\theta)+(\cos^2\psi)(\sin^2\theta)J_2(d\sin\theta)\right]\sqrt{\frac{\pi}{2}}\sqrt{c\cos\theta}J_{-1/2}(c\cos\theta) \\
&= \sqrt{\frac{\pi^3}{2}}\left[\frac{1}{(kR)^{1/2}}J_{1/2}(kR)-\frac{1}{(kR)^{3/2}}J_{3/2}(kR)+\cos^2\psi\frac{d^2}{(kR)^{5/2}}J_{5/2}(kR)\right] \\
&= \pi\left\{\frac{\sin kR}{kR}\left(1-\frac{y_B^2}{R^2}\right)+\left[\frac{\cos kR}{(kR)^2}-\frac{\sin kR}{(kR)^3}\right]\left(1-\frac{3y_B^2}{R^2}\right)\right\}. \qquad \text{(C9)}
\end{aligned}
$$

Here in deriving the second equation we have used the recurrence formula for the Bessel functions [52]. The integral in the third equation has been performed using the second Sonine's formula [52]. Finally, in going from the forth equation to the fifth, we have rewritten the Bessel functions of half-integer order in terms of elementary functions [52]. The distance R stands for R_{rn} if $c=c_r$ and R_{ln} if $c=c_l$, see Eqs. (43) and (C5).

Now by inserting Eqs. (C9) in (C3) and performing the integration over k in the same way as in Eq. (A6), we arrive at Eqs. (42), (43), and (44b) for $F_y(\mathbf{r}_B,\mathbf{r}_A,t)$. Other components and the case of a z-oriented dipole can be treated in the same manner.

[1] *Spontaneous Emission and Laser Oscillation in Microcavities*, edited by H. Yokoyama and K. Ujihara (CRC, Boca Raton, Florida, 1995).
[2] *Cavity Quantum Electrodynamics*, edited by P. R. Berman (Academic, New York, 1994).
[3] E. A. Hinds, in *Advances in Atomic, Molecular, and Optical Physics*, edited by D. Bates and B. Bederson (Academic, New York, 1991), Vol. 28, p. 237.
[4] F. De Martini and G. R. Jacobovitz, Phys. Rev. Lett. **60**, 1711 (1988).
[5] H. Yokoyama and S. D. Brorson, J. Appl. Phys. **66**, 4801 (1989).
[6] Y. Yamamoto, S. Machida, and G. Björk, Phys. Rev. A **44**, 657 (1991).
[7] I. Takahashi and K. Ujihara, Opt. Commun. **158**, 331 (1998).
[8] M. Ley and R. Loudon, J. Mod. Opt. **34**, 227 (1987).
[9] K. Ujihara, IEEE J. Quantum Electron. **24**, 1367 (1988).
[10] H. Khosravi and R. Loudon, Proc. R. Soc. London, Ser. A **436**, 373 (1992).
[11] M. R. Philpott, Chem. Phys. Lett. **19**, 435 (1973).
[12] G. Barton, Proc. R. Soc. London, Ser. A **320**, 251 (1970).
[13] R. G. Hullet, E. S. Hilfer, and D. Kleppner, Phys. Rev. Lett. **55**, 2137 (1985).
[14] S. D. Brorson, Y. Yokoyama, and E. P. Ippen, IEEE J. Quantum Electron. **26**, 1492 (1990).
[15] K. Ujihara, Jpn. J. Appl. Phys., Part 2 **30**, L901 (1991).
[16] K. Ujihara, A. Nakamura, O. Manba, and X.-P. Feng, J. Appl. Phys. **30**, 3388 (1991).
[17] F. De Martini, M. Marrocco, P. Mataloni, L. Crescentini, and R. Loudon, Phys. Rev. A **43**, 2480 (1991).
[18] G. Björk, S. Machida, Y. Yamamoto, and K. Igeta, Phys. Rev. A **44**, 669 (1991).
[19] Y. Yamamoto, S. Machida, and G. Björk, Opt. Quantum Electron. **24**, S215 (1992).
[20] G. Björk, IEEE J. Quantum Electron. **30**, 2314 (1994).
[21] S. M. Dutra and P. L. Knight, Phys. Rev. A **53**, 3587 (1996).
[22] I. Abram, I. Robert, and R. Kuszelewicz, IEEE J. Quantum Electron. **34**, 71 (1998).
[23] R. J. Cook and P. W. Milonni, Phys. Rev. A **35**, 5081 (1987).
[24] X.-P. Feng and K. Ujihara, IEEE J. Quantum Electron. **25**, 2332 (1989).
[25] X.-P. Feng and K. Ujihara, Phys. Rev. A **41**, 2668 (1990).
[26] H. Gießen, J. D. Berger, G. Mohs, P. Meystre, and S. F. Yelin, Phys. Rev. A **53**, 2816 (1996).
[27] I. Takahashi and K. Ujihara, Phys. Rev. A **56**, 2299 (1997).
[28] E. T. Jaynes and F. W. Cummings, Proc. IEEE **51**, 89 (1963).
[29] J. J. Sanchez-Mondragon, N. B. Narozhny, and J. H. Eberly, Phys. Rev. Lett. **51**, 550 (1983).
[30] F. De Martini, M. Marrocco, and D. Murra, Phys. Rev. Lett. **65**, 1583 (1990).
[31] A. Takada and K. Ujihara, Opt. Commun. **160**, 146 (1999).
[32] T. Baba and K. Iga, in *Spontaneous Emission and Laser Oscillation in Microcavities*, edited by H. Yokoyama and K. Ujihara (CRC, Boca Raton, Florida, 1995) p. 237.
[33] P. W. Milonni and P. L. Knight, Opt. Commun. **9**, 119 (1973).
[34] J. P. Dowling, M. O. Scully, and F. De Martini, Opt. Commun. **82**, 415 (1991).
[35] M. Höijer and G. Björk, Opt. Commun. **150**, 319 (1998).
[36] R. H. Lehmberg, Phys. Rev. A **2**, 883 (1970).
[37] P. W. Milonni and P. L. Knight, Phys. Rev. A **11**, 1090 (1975).
[38] H. T. Dung and K. Ujihara, Phys. Rev. A **59**, 2524 (1999).
[39] C. Cohen-Tannoudji, J. Dupont-Roc, and G. Grynberg, *Photons and Atoms: Introduction to Quantum Electrodynamics* (Wiley, New York, 1989).
[40] H. J. Carmichael, R. J. Brecha, M. G. Raizen, H. J. Kimble, and P. R. Rice, Phys. Rev. A **40**, 5516 (1989).
[41] E. V. Goldstein and P. Meystre, in *Spontaneous Emission and*

Laser Oscillation in Microcavities, edited by H. Yokoyama and K. Ujihara (CRC, Boca Raton, Florida, 1995) p. 2.
[42] L. V. Ahlfors, *Complex Analysis* (McGraw-Hill, New York, 1953) p. 149.
[43] A. Ueda, N. Uehara, and K. Ueda, Opt. Rev. **3**, 369 (1996).
[44] T. B. Norris, J.-K Rhee, C.-Y Sung, Y. Arakawa, M. Nishioka, and C. Weisbuch, Phys. Rev. B **50**, 14 663 (1994).
[45] C. Weisbuch, M. Nishioka, A. Ishikawa, and Y. Arakawa, Phys. Rev. Lett. **69**, 3314 (1992).
[46] M. S. Skolnick, T. A. Fisher, and D. M. Whittaker, Semicond. Sci. Technol. **13**, 645 (1998).
[47] Y. Kaluzny, P. Goy, M. Gross, J. M. Raimond, and S. Haroche, Phys. Rev. Lett. **51**, 1175 (1983); M. G. Raizen, R. J. Thompson, R. J. Brecha, H. J. Kimble, and H. J. Carmichael, *ibid.* **63**, 240 (1989).
[48] E. Hanamura, Phys. Rev. B **38**, 1228 (1988).
[49] M. Born and E. Wolf, *Principle of Optics* (Pergamon, Oxford, 1980).
[50] T. Enomoto, T. Sasaki, K. Sekiguchi, Y. Okada, and K. Ujihara, J. Appl. Phys. **80**, 6595 (1996).
[51] E. Hairer, S. P. Norsett, and G. Wanner, *Solving Ordinary Differential Equations I: Nonstiff Problems* (Springer-Verlag, Berlin, 1993).
[52] G. N. Watson, *A Treatise on the Theory of Bessel Functions* (Cambridge University Press, Cambridge, England, 1966).